AIAA SciTech Forum
12-16 January 2026, Orlando, FL
AIAA SCITECH 2026 Forum

10.2514/6.2026-1699

Trade Study of Regular and Flapped CoFlow Jet Airfoils, Part I: Injection Slot Size Effect

Feihao Ding * Jaehyoung Jeon † Gecheng Zha ‡
Dept. of Mechanical and Aerospace Engineering
University of Miami, Coral Gables, Florida 33124

Abstract

This paper conducts a trade study of injection sizes for regular CoFlow Jet (CFJ) (RCFJ) airfoil and flapped CoFlow Jet (FCFJ) airfoil. Three injection slot sizes, 0.4%C, 0.65%C, and 1.15%C, are studied under Martian low Reynolds number condition of $Re = 5.6 \times 10^4$ and Earth high Reynolds number condition of $Re = 1.0 \times 10^6$ at $M_\infty = 0.17$. The FCFJ airfoil has the injection positioned at the flap shoulder, whereas the RCFJ has the injection located at about 2% chord from the leading edge. For all the slot sizes and Reynolds numbers, the RCFJ airfoil demonstrates better aerodynamic efficiency over most of the lift coefficient range. For C_L below about 5–7, the RCFJ airfoil exhibits lower drag coefficient C_D, and a lower coefficient of power required P_c, and higher corrected aerodynamic efficiency $(C_L/C_D)_c$ and $(C_L^2/C_D)_c$ than the FCFJ airfoil. For $C_L \geq 7$, the FCFJ airfoil has better aerodynamic efficiency and can achieve comparable or lower P_c at higher lift. When the injection slot is choked with the injection Mach number of 1 or greater, the CFJ power coefficient increases exponentially with C_L due to the rapidly increased jet total pressure ratio to overcome the high energy loss at high injection speed. For corrected aerodynamic efficiency $(C_L/C_D)_c$, all three injection slot sizes have a similar peak value for both configurations. However, the injection slot size has a stronger effect on the productivity efficiency $(C_L^2/C_D)_c$ on the FCFJ airfoil than on the RCFJ airfoil. For the FCFJ airfoil, the 0.4%C slot yields the highest peak productivity efficiency of $(C_L^2/C_D)_c = 50.5$ at low Reynolds number, whereas the $(C_L^2/C_D)_c$ for 1.15%C slot decreases 25.9%. In contrast, the RCFJ shows less sensitivity on productivity efficiency to slot size, with peak $(C_L^2/C_D)_c$ decreases only 15.0% from 0.65% slot size to 0.4% slot size. Increasing Reynolds number substantially improves the corrected aerodynamic efficiency and productivity efficiency for both the configurations, with peak $(C_L/C_D)_c$ and $(C_L^2/C_D)_c$ values both increase about 100%. Increasing the Reynolds number also reduces both airfoils' sensitivity on the injection slot sizes. These results suggest that RCFJ airfoils are better suited for efficient cruise and moderate-lift coefficient (e.g., $C_L < 7$) operation, whereas FCFJ airfoils provide a more efficient option for ultra-high-lift applications such as short or vertical takeoff and landing.

Nomenclature

CFJ	CoFlow jet

* Ph.D. Candidate
† Ph.D. Student
‡ Professor, ASME Fellow, AIAA associate Fellow

$RCFJ$	Regular CoFlow jet
$FCFJ$	Flapped CoFlow jet
$AoA(\alpha)$	Angle of attack
β	Deflection angle
LE	Leading Edge
TE	Trailing Edge
s	Wing Span length
c	Profile chord
U	Flow velocity
q	Dynamic pressure $0.5\,\rho\,U^2$
p	Static pressure
ρ	Air density
P	Pumping power
C_L	Lift coefficient $L/(q_\infty\,S)$
C_D	Drag coefficient $D/(q_\infty\,S)$
C_μ	Jet momentum coef. $\dot{m}_j\,U_j/(q_\infty\,S)$
Pc	Power coefficient $P/(q_\infty\,S\,V_\infty)$
$(C_L/C_D)_c$	CFJ airfoil corrected efficiency $C_L/(C_D$+Pc)
$(C_L^2/C_D)_c$	CFJ airfoil productivity efficiency $C_L^2/(C_D + P/V_\infty)$
R_e	Reynolds number
M	Mach number
c_p	Constant pressure specific heat
γ	Air specific heats ratio
S	Planform area of the wing
T_t	Total temperature
P_t	Total pressure
H_t	Total specific enthalpy
$\dot{m}$	Mass flow across the pump
$_\infty$	Subscript, stands for free stream
$_j$	Subscript, stands for jet

1 Introduction

High aerodynamic efficiency leads to reduced fuel consumption, operating costs, and greenhouse gas emissions. This has become increasingly important as the aviation industry seeks more sustainable solutions. To achieve better aerodynamic performance, engineers have developed various airfoil configurations. Regular airfoils and flapped airfoils each have their distinct advantages. Regular airfoils are used for cruise, whereas flapped airfoils are typically used for high lift enhancement or control surfaces. Driven by fixed-wing VTOL aircraft using deflected slipstream and the flight on Martian low-density environment, flapped airfoils with CoFlow Jet active flow control are utilized for the entire flight envelope that includes hover, transition, and cruise [1, 2].

Active Flow Control (AFC) energizes airflow to enhance aerodynamic performance, such as increasing lift, stall margin, and reducing drag. Typical AFC systems inject or remove air at effective locations on the airfoil surface. This added energy helps to keep the flow attached and improve overall circulation.

Yet, integrating AFC into aircraft operations for the entire flight envelope presents various challenges. A crucial condition for an AFC to be viable is that the aerodynamic benefits must outweigh its energy costs.

A promising AFC technology with the potential to enhance mission efficiency through the entire flight envelope is the CoFlow Jet (CFJ) flow control airfoil recently developed [3, 4, 5, 6, 7, 8, 9, 10, 11, 12, 13, 14, 15, 16, 17, 18]. The mechanism of the CFJ airfoil relies on a series of micro-compressor actuators embedded inside the wing along the span, injecting jets of high-momentum fluid parallel to the airfoil surface, and withdrawing the same amount of mass flow downstream. Such a flow mechanism embeds the entire CFJ in the adverse pressure gradient region to be efficient and effective [18, 19]. This injection and suction process creates a self-contained zero-net-mass-flux flow control with low energy expenditure. Fig. 1 illustrates the concept of a regular CFJ airfoil. It has the injection near the leading edge and suction near the trailing edge. For an RCFJ to increase lift coefficient, the wing or the aircraft needs to rotate nose-up to increase the angle of attack (AoA).

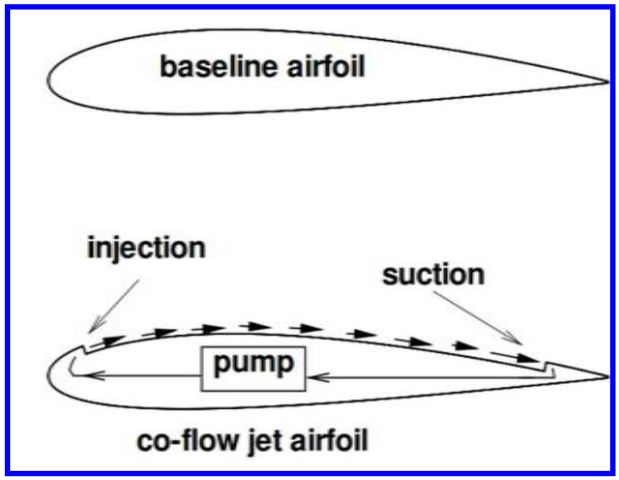

Figure 1: Sketch of CoFlow Jet airfoil

1.1 Flapped CoFlow Jet Airfoil

The concept of a flapped coflow jet airfoil is developed to achieve a deflected slipstream for VTOL aircraft [20, 2]. The CFJ is applied inside a flap, as illustrated in Fig. 2 [21], which has the injection located at the shoulder of the flap. The advantage of an FCFJ airfoil is that it can increase lift coefficient by only deflecting the flap with the front part fixed without rotating the whole wing. This fosters the concept of VTOL aircraft using deflected slipstream [1, 2], which does not need to tilt the propellers facing upward as conventional rotorcraft.

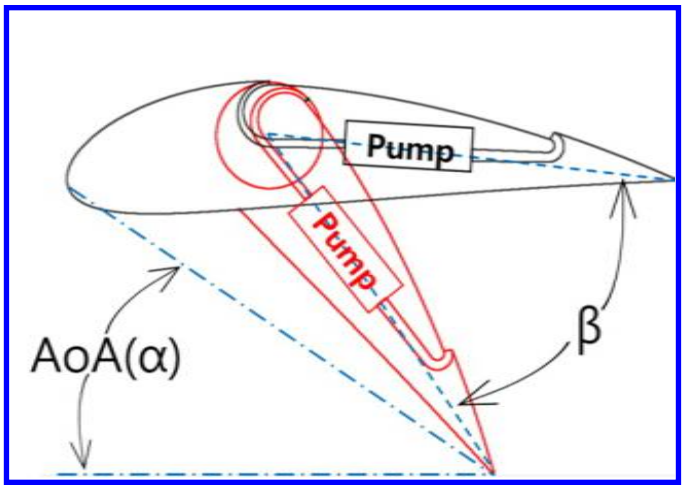

Figure 2: Sketch of flapped CFJ airfoil with the CoFlow jet applied on the flap

The objective of this paper is to conduct a trade study and comparison of the aerodynamic performance of two CoFlow Jet airfoil configurations: the Regular CoFlow Jet airfoil and the Flapped CoFlow Jet airfoil. The study will compare how these two CFJ configurations, under both Martian (low Reynolds number) and Earth (high Reynolds number) conditions, respond to variations in injection slot size while keeping a fixed suction slot size and the same C_L conditions. The performance of these two airfoils is compared from cruise condition at low AoA and low C_L to high lift condition and high AoA with C_L up to around 8.5.

2 Methodology

2.1 Lift and Drag Calculation

In the CFD analysis, the total aerodynamic forces and moments are determined from the surface pressure and shear stress distributions, together with the jet reaction forces generated by the CFJ system. The reaction forces are obtained using the flow parameters at the injection and suction slots based on the control-volume method illustrated in Fig. 3. The governing equations for the CFJ jet reaction forces are expressed as [4]:

$$F_{x_{cfj}} = (\dot{m}_1 V_{j1} + p_{j1} A_{j1}) \cos(\theta_1 - \alpha) - (\dot{m}_2 V_{j2} + p_{j2} A_{j2}) \cos(\theta_2 + \alpha) \tag{1}$$

$$F_{y_{cfj}} = (\dot{m}_1 V_{j1} + p_{j1} A_{j1}) \sin(\theta_1 - \alpha) + (\dot{m}_2 V_{j2} + p_{j2} A_{j2}) \sin(\theta_2 + \alpha) \tag{2}$$

Here, subscripts 1 and 2 denote the injection and suction slots, respectively. The terms θ_1 and θ_2 represent the angles between each slot surface and a line normal to the chord, and α is the angle of attack. The mass flow rate $\dot{m}$, jet velocity V_j, static pressure p_j, and slot area A_j are evaluated at each slot exit or inlet.

The total aerodynamic lift and drag are then obtained by combining the surface pressure–shear integrals with the CFJ reaction forces:

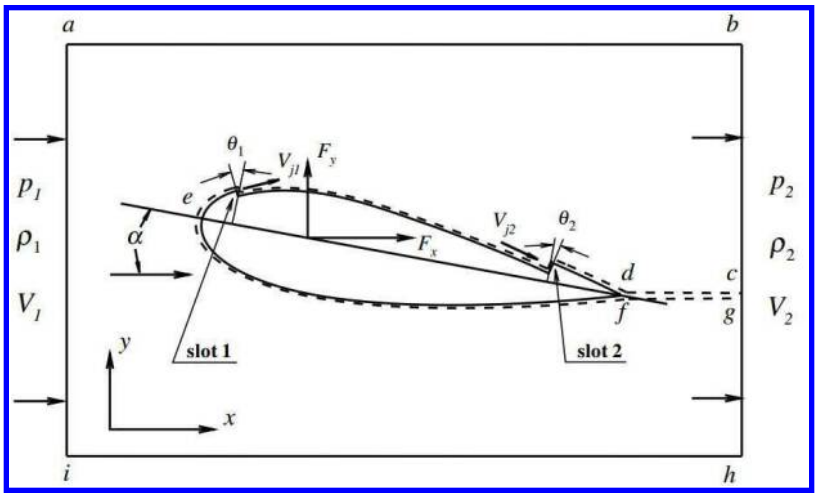

Figure 3: Control volume of a CFJ airfoil

$$D = R'_x - F_{x_{cfj}} \tag{3}$$

$$L = R'_y - F_{y_{cfj}} \tag{4}$$

where R'_x and R'_y are the net pressure and shear contributions in the drag and lift directions, respectively. For 3D CFJ wings, the total lift and drag are obtained by integrating these quantities in the spanwise direction.

2.2 Jet Momentum Coefficient

The jet momentum coefficient C_μ is a parameter used to quantify the jet intensity. It is defined as:

$$C_\mu = \frac{\dot{m} V_j}{\frac{1}{2}\rho_\infty {V_\infty}^2 S} \tag{5}$$

where $\dot{m}$ is the injection mass flow, V_j is the mass-averaged injection velocity, ρ_∞ and V_∞ denote the free stream density and velocity, and S is the planform area.

2.3 Micro-compressor Power Coefficient

CFJ is implemented by mounting a pumping system inside the wing that withdraws air from the suction slot and blows it into the injection slot. The power consumption is determined by the jet mass flow and total enthalpy change as follows:

$$P = \dot{m}(H_{t1} - H_{t2}) \tag{6}$$

where H_{t1} and H_{t2} are the mass-averaged total enthalpy in the injection cavity and suction cavity respectively, P is the Power required by the pump and $\dot{m}$ the jet mass flow rate. Introducing P_{t1} and P_{t2}

the mass-averaged total pressure in the injection and suction cavity respectively, the compressor efficiency η, and the total pressure ratio of the pump $\Gamma = \frac{P_{t1}}{P_{t2}}$, the power consumption is expressed as:

$$P = \frac{\dot{m} C_p T_{t2}}{\eta} (\Gamma^{\frac{\gamma-1}{\gamma}} - 1) \tag{7}$$

where γ is the specific heat ratio equal to 1.4 for air. The power coefficient is expressed as:

$$P_c = \frac{P}{\frac{1}{2}\rho_\infty V_\infty^3 S} \tag{8}$$

2.4 Aerodynamic Efficiency

The conventional wing aerodynamic efficiency is defined as:

$$\frac{C_L}{C_D} \tag{9}$$

For the CFJ wing, the ratio above still represents the pure aerodynamic relationship between lift coefficient and drag coefficient. However, since CFJ active flow control consumes energy, the ratio above is modified to take into account the energy consumption of the micro-compressor. The formulation of the corrected aerodynamic efficiency for CFJ wings is:

$$(\frac{C_L}{C_D})_c = \frac{C_L}{C_D + P_c} \tag{10}$$

where P_c is the micro-compressor power coefficient defined in Eqn. 8 and C_L and C_D are the lift and drag coefficients of the CFJ wing. If the micro-compressor power coefficient is set to 0, this formulation returns to the aerodynamic efficiency of a conventional airfoil.

A productivity efficiency parameter was introduced by Yang et al[14]. It describes the capability to transport a gross weight for a maximum distance at cruise:

$$(\frac{C_L^2}{C_D})_c = \frac{C_L^2}{C_D + P_c} \tag{11}$$

2.5 CFD Simulation Setup

The FASIP(Flow-Acoustics-Structure Interaction Package) CFD code is used to conduct the numerical simulation. The 2D Reynolds Averaged Navier-Stokes (RANS) equations with one-equation Spalart-Allmaras (SA) turbulence model are used. A 3rd order WENO scheme for the inviscid flux [22, 23, 24, 25, 26, 27] and a 2nd order central differencing for the viscous terms [22, 26] are employed to discretize the Navier-Stokes equations. The low diffusion E-CUSP scheme used as the approximate Riemann solver suggested by Zha et al [23] is utilized with the WENO scheme to evaluate the inviscid fluxes. Implicit time marching method using Gauss-Seidel line relaxation is used to achieve a fast convergence rate [28].

Parallel computing is implemented to save wall clock simulation time [29]. The FASIP CFD code and numerical algorithms are intensively validated with CFJ flows. [4, 7, 30, 31, 32, 19]

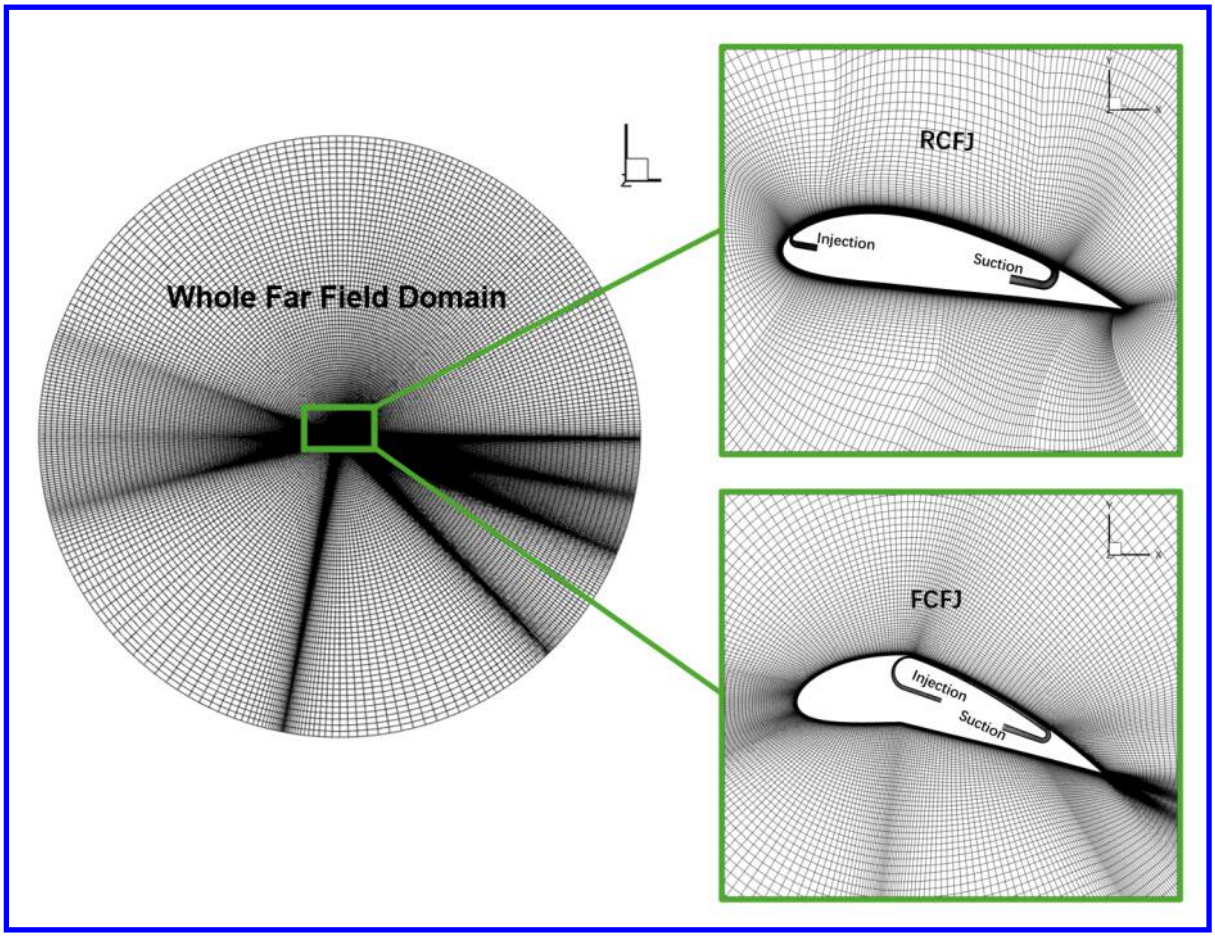

Figure 4: Computational mesh used in the current work.

2.6 Boundary Conditions and Mesh Analysis

The 3rd-order accuracy no-slip condition is enforced on the solid surface with the wall treatment suggested in [33] to achieve the flux conservation on the wall. The far-field boundary is located at 250 chords with an O-mesh topology. The computational mesh is shown in Fig. 4. The free-stream conditions of $Ma = 0.17$, $Re = 56,300$, and $Re = 1 \times 10^6$ are used in this study to simulate Martian and Earth conditions correspondingly. Constant static pressure is applied at the downstream portion of the far field. The first grid point on the wing surface is placed at $y^+ \approx 1$.

3 Airfoil Geometry Parameters

The specific parameters of the airfoils based on the NACA 6421 baseline with the injection and suction slot size normalized by airfoil chord length (C) are given in Table. 1. The RCFJ airfoil adopts the CFJ6421-SST150-SUC133 optimized by Lefebvre and Zha [16] for its high lift and cruise efficiency. The

FCFJ airfoil is modified from the CFJ6421-SST150-SUC133 airfoil with a flap length of about 60%C, which keeps the suction surface translation (SST) of 1.50%C and suction slot size of 1.33%C and location identical to the RCFJ airfoil. In this study, the AoA of the RCFJ airfoil is varied from 5° to 45° to cover the range from cruise to high lift conditions with C_L varying from 1.067 to 8.239. The FCFJ airfoil has the flap deflection β varied from 5° to 75°, which has the AoA varying from 3.3° to 54° to achieve a similar C_L range as that of the RCFJ airfoil.

Table 1: Airfoil geometry parameters

Airfoil	Angle of Attack (AoA)	Deflection Angle (β)	SST(%C)	INJ(%C)	SUC(%C)
RCFJ	5° - 45°	N/A	1.5	0.4, 0.65, 1.15	1.33
FCFJ	3.3° - 54°	5° - 75°	1.5	0.4, 0.65, 1.15	1.33

4 Results and Discussion

To investigate the effect of jet sizing, three different injection slot sizes are studied: 0.4%C, 0.65%C, and 1.15%C. The simulations are conducted under two flow conditions. The first condition corresponds to the Martian low speed environment with a Reynolds number of $Re = 5.6 \times 10^4$ and a freestream Mach number of $M_\infty = 0.17$. The second one represents an Earth condition with $Re = 1.0 \times 10^6$ at the same Mach number.

To evaluate the performance from efficient cruise to high lift conditions, the RCFJ is simulated across a range of jet momentum coefficients from $C_\mu = 0.01$ to $C_\mu = 1.0$ and angles of attack from $\alpha = 5°$ to $\alpha = 45°$, while the FCFJ is simulated across the same range of C_μ and flap deflection angles from $\beta = 5°$ to $\beta = 75°$. The aerodynamic performance metrics, including drag coefficient (C_D), power coefficient (P_c), CFJ total pressure ratio (P_{tr}), Angle of attack (AoA), jet momentum coefficient (C_μ), Mach number at injection (M_{inj}), aerodynamic efficiency (C_L/C_D), corrected aerodynamic efficiency ($(C_L/C_D)_c$), and productivity efficiency ($(C_L^2/C_D)_c$) are compared with respect to the lift coefficient (C_L) for all configurations. Specifically, for each configuration and each C_L value, the $C\mu$ and α or β are iterated to achieve the highest $(C_L/C_D)_c$ and $(C_L^2/C_D)c$. The case is then selected for comparison.

Fig. 5 shows the flow fields and pressure coefficient (C_p) distributions of the low Reynolds number cases for the RCFJ and FCFJ airfoil at the C_L of about 1.5 with C_μ of 0.04. Both flows are well attached. For the RCFJ airfoil, the C_p peak occurs immediately at downstream of the leading edge. The peak of C_p for the FCFJ airfoil is located at the flap shoulder position with a higher value, which results in a higher adverse pressure gradient.

Fig. 6 illustrates the zoomed-in flow fields near the injection outlet and the corresponding pressure coefficient C_p distributions at a high lift coefficient $C_L = 5$ with AoA of 40° for the RCFJ airfoil and β of 40° for the FCFJ airfoil. The Mach contours indicate that the flow is choked at the injection slot. For both configurations, the C_p peaks are located at the injection outlet. The RCFJ airfoil exhibits a sharp decrease of $-C_p$ in adverse pressure gradient (APG) immediately downstream of this peak. The FCFJ airfoil achieves the first APG area immediately downstream of the leading edge, and the second APG area at the shoulder of the flap. Compared to the $C_L = 1.5$ case, the overall magnitude of C_p is significantly increased.

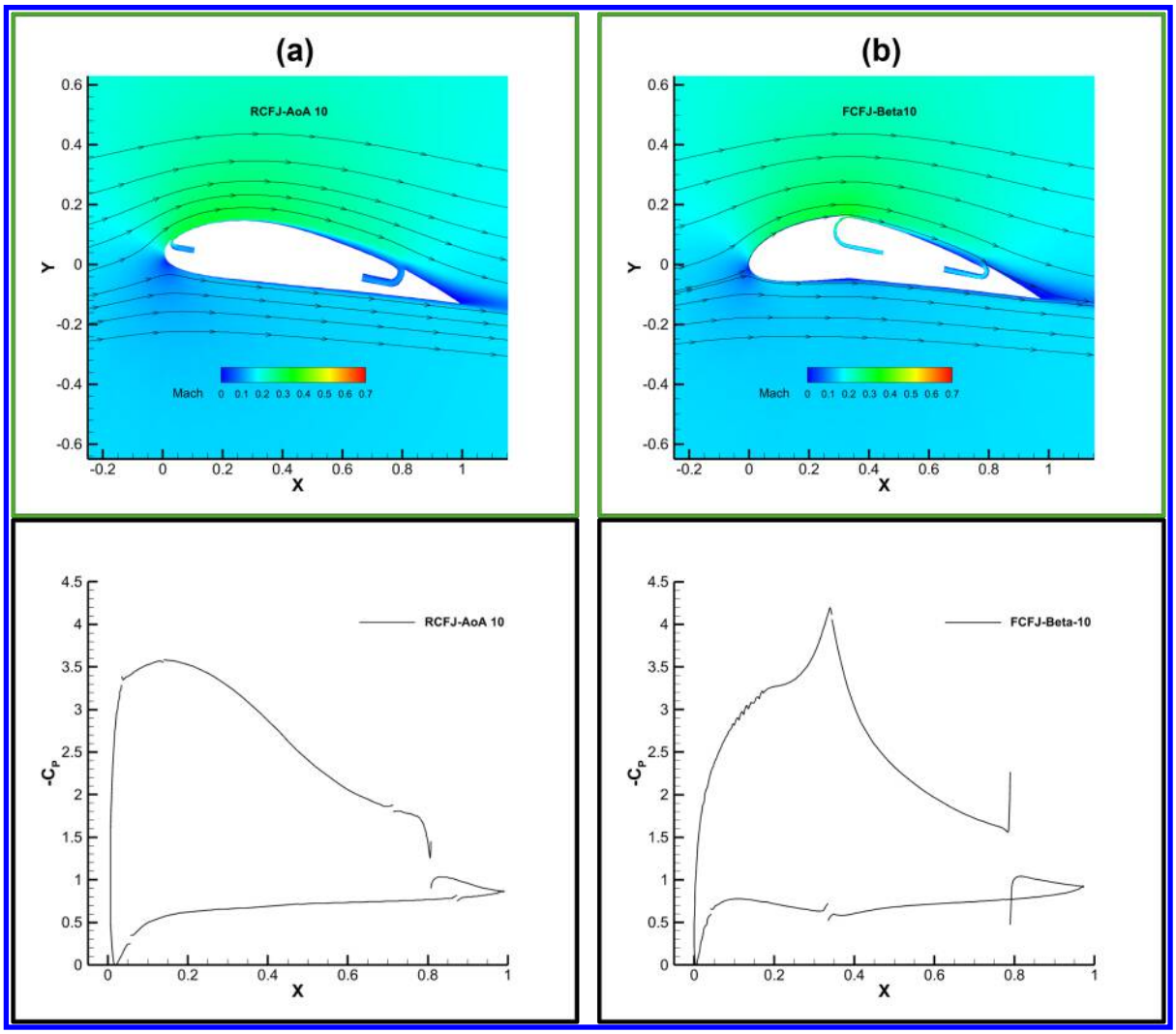

Figure 5: Flow fields at surface pressure coefficient distributions at $C_L \approx 1.5$, AoA$= 10^\circ$ for RCFJ airfoil, $\beta = 10^\circ$ for FCFJ airfoil.

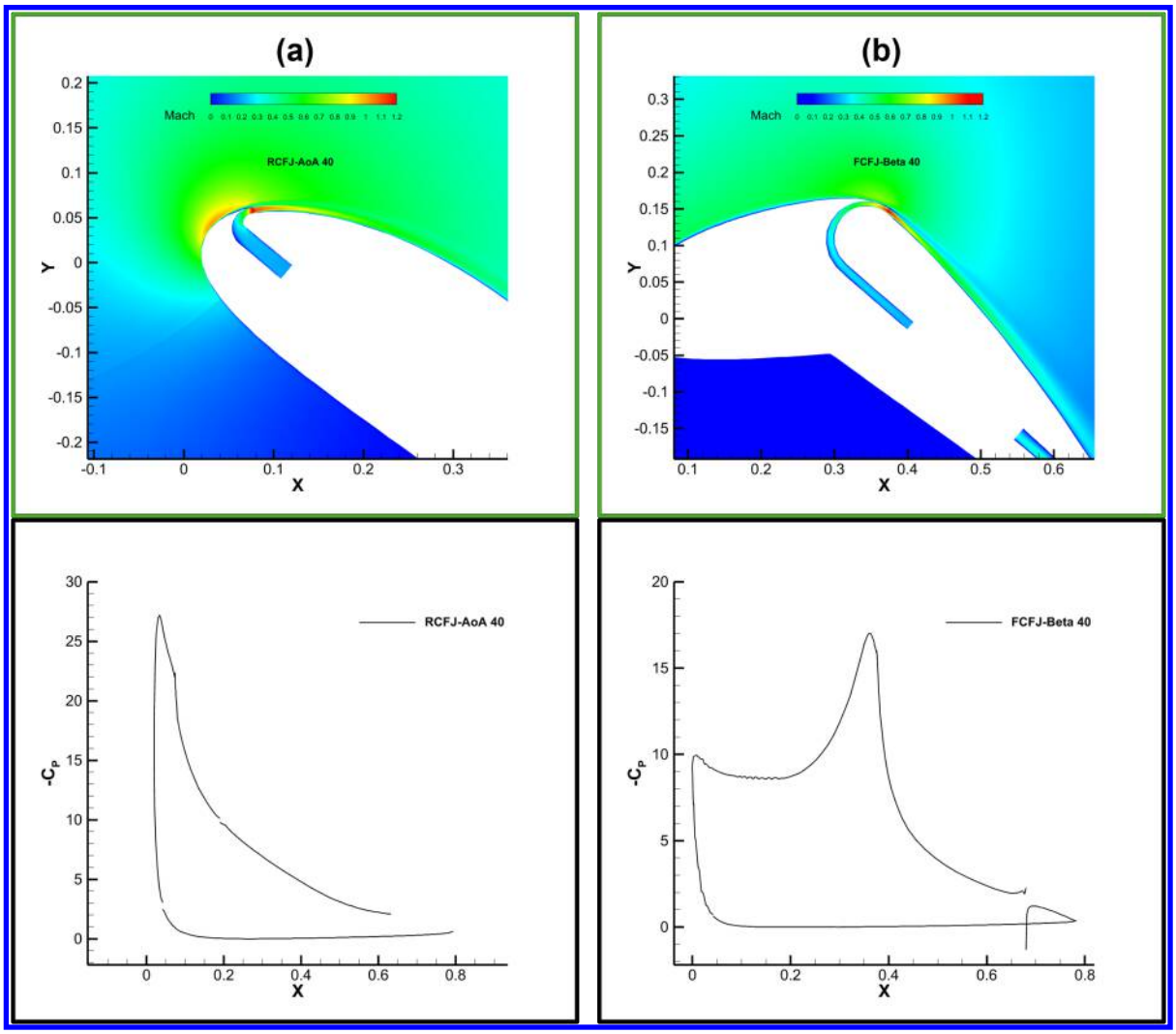

Figure 6: Flow fields at surface pressure coefficient distributions at $C_L \approx 5.0$, AoA= 40° for RCFJ airfoil, β= 40° for FCFJ airfoil.

4.1 Low Reynolds Number Case

Figures 7–9 compare the RCFJ and FCFJ configurations at $Re = 5.6 \times 10^4$ for the three injection slot sizes of $0.4\%C$, $0.65\%C$, and $1.15\%C$. In all cases, each data point corresponds to a different combination of C_μ and geometric setting (α for RCFJ and β for FCFJ), but the results are plotted as a function of lift coefficient C_L to enable direct comparison. The aerodynamic performance metrics of C_D, P_c, Ptr, AoA, C_μ, M_{inj}, C_L/C_D, $(C_L/C_D)_c$, and $(C_L^2/C_D)_c$ are given in the figures.

In Fig. 7, the M_{inj} shows that the injection velocity becomes plateaued when the C_L reaches about 4 and 5, respectively, for the RCFJ airfoil and FCFJ airfoil with an injection slot size of 0.4%C. The injection Mach number is plateaued at about 1 for the RCFJ airfoil and about 1.1 for the FCFJ airfoil due to a slight converging-diverging shape upstream of the FCFJ airfoil injection slot. The injection jet further accelerates supersonically immediately downstream of the injection slot, and then decays quickly due to mixing with the main flow in APG, as shown in Fig. 6. The high-speed supersonic jet creates a high energy

loss as the total pressure ratio Pt_r increases dramatically after the injection slot is choked. Since the CFJ power is determined by the Pt_r exponentially, the CFJ power coefficient P_c increases exponentially when the injection slot is choked. Such a phenomenon occurs for all the configurations studied in this paper. For aerodynamic efficiency and productivity efficiency, the RCFJ airfoil demonstrates a clear advantage across all slot sizes at $C_L \leq 7$. For a given C_L, the RCFJ airfoil exhibits lower C_D, lower power coefficient P_c, and lower compressor pressure ratio compared with the FCFJ airfoil. However, when C_L increases above 7, the power required for the FCFJ airfoil becomes substantially lower than that for the RCFJ airfoil. This further demonstrates that the flapped configuration is more effective for high lift situations.

Since the drag coefficient C_D of a CFJ airfoil can become very small, zero, or negative, the C_L/C_D can be very large or negative. When the C_D is zero or negative, the aircraft is able to fly by CFJ itself without using separate propulsion systems. To compare with conventional aerodynamic efficiency, the corrected aerodynamic efficiency defined in Eq. 10 should be used to include the power consumed by the CFJ system.

The corrected aerodynamic efficiency $(C_L/C_D)_c$ and productivity efficiency $(C_L^2/C_D)_c$ show a consistent trend across all three injection slot sizes: the RCFJ performs better in the range of lower lift coefficient with $C_L < 5$ for the two small injection size of $0.4\%C$ and $0.65\%C$, whereas the FCFJ airfoil is more efficient above that threshold. For the larger injection slot size of 1.15%, the threshold is about $C_L = 7$.

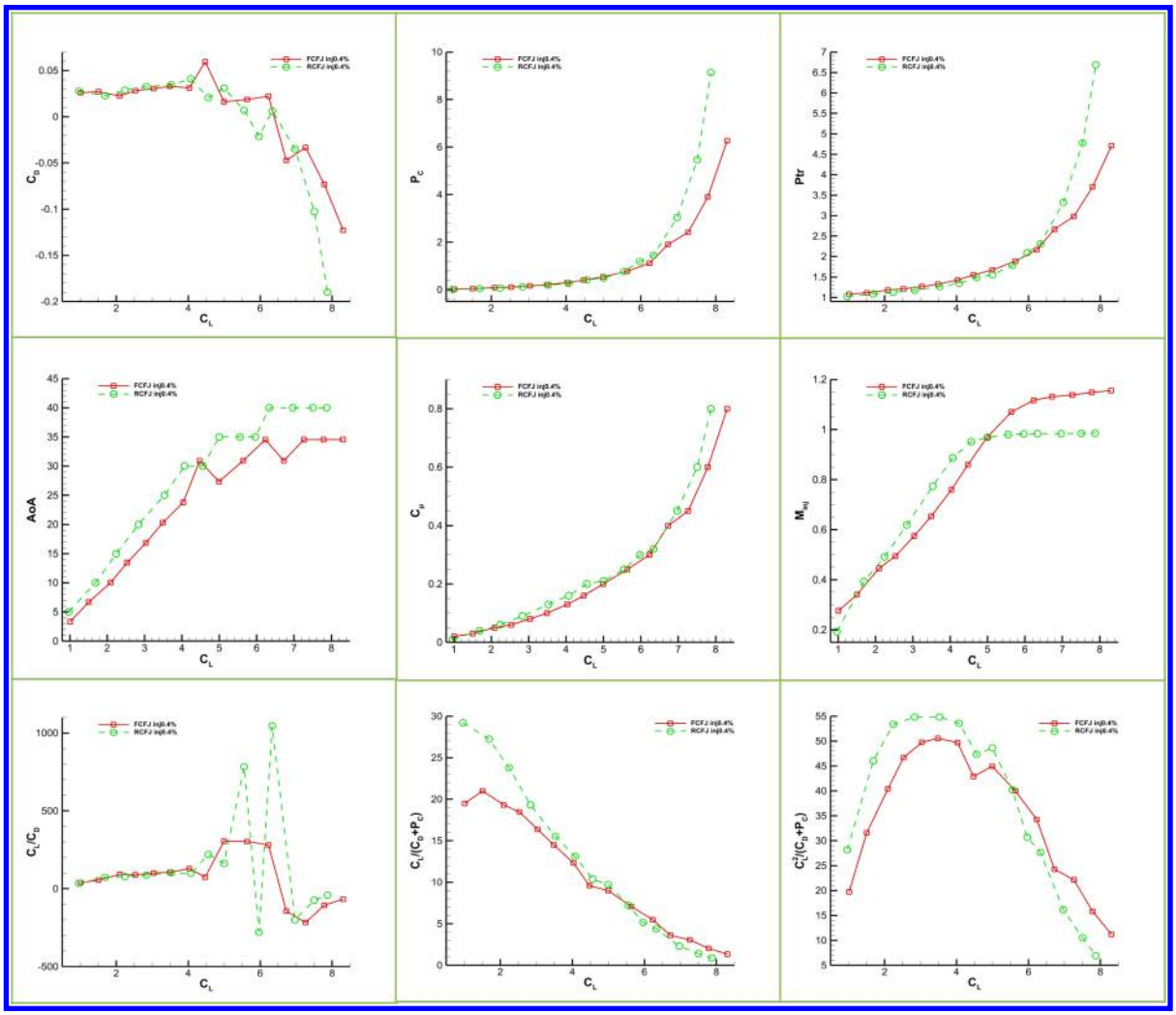

Figure 7: Comparison of C_D, P_c, Ptr, AoA, C_μ, M_{inj}, C_L/C_D, $(C_L/C_D)_c$, $(C_L^2/C_D)_c$ for RCFJ and FCFJ airfoils with $0.4\%C$ injection slot size at $Re = 56,300$

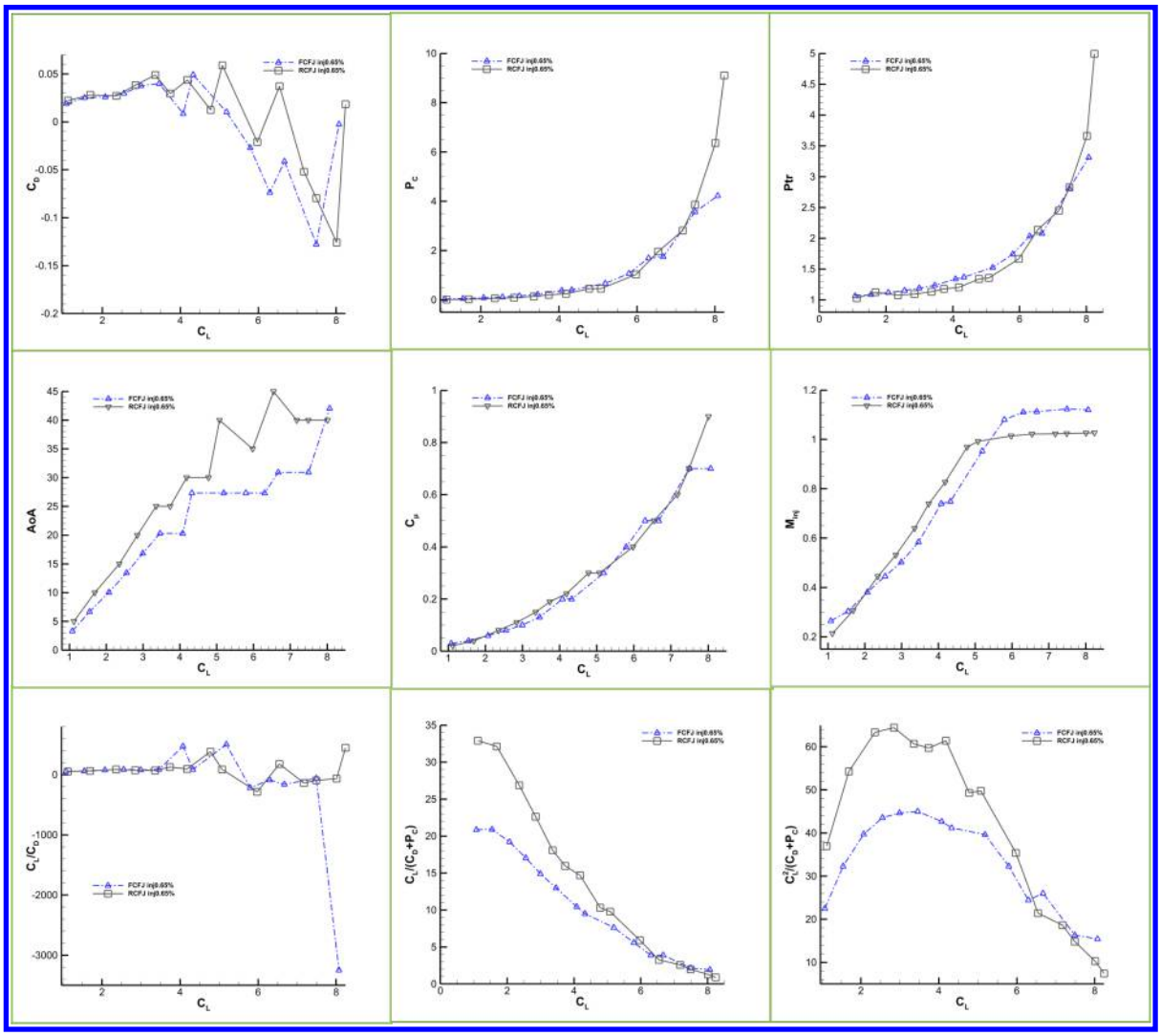

Figure 8: Comparison of C_D, P_c, Ptr, AoA, C_μ, M_{inj}, C_L/C_D, $(C_L/C_D)_c$, $(C_L^2/C_D)_c$ for RCFJ and FCFJ airfoils with $0.65\%C$ injection slot size at $Re = 56,300$.

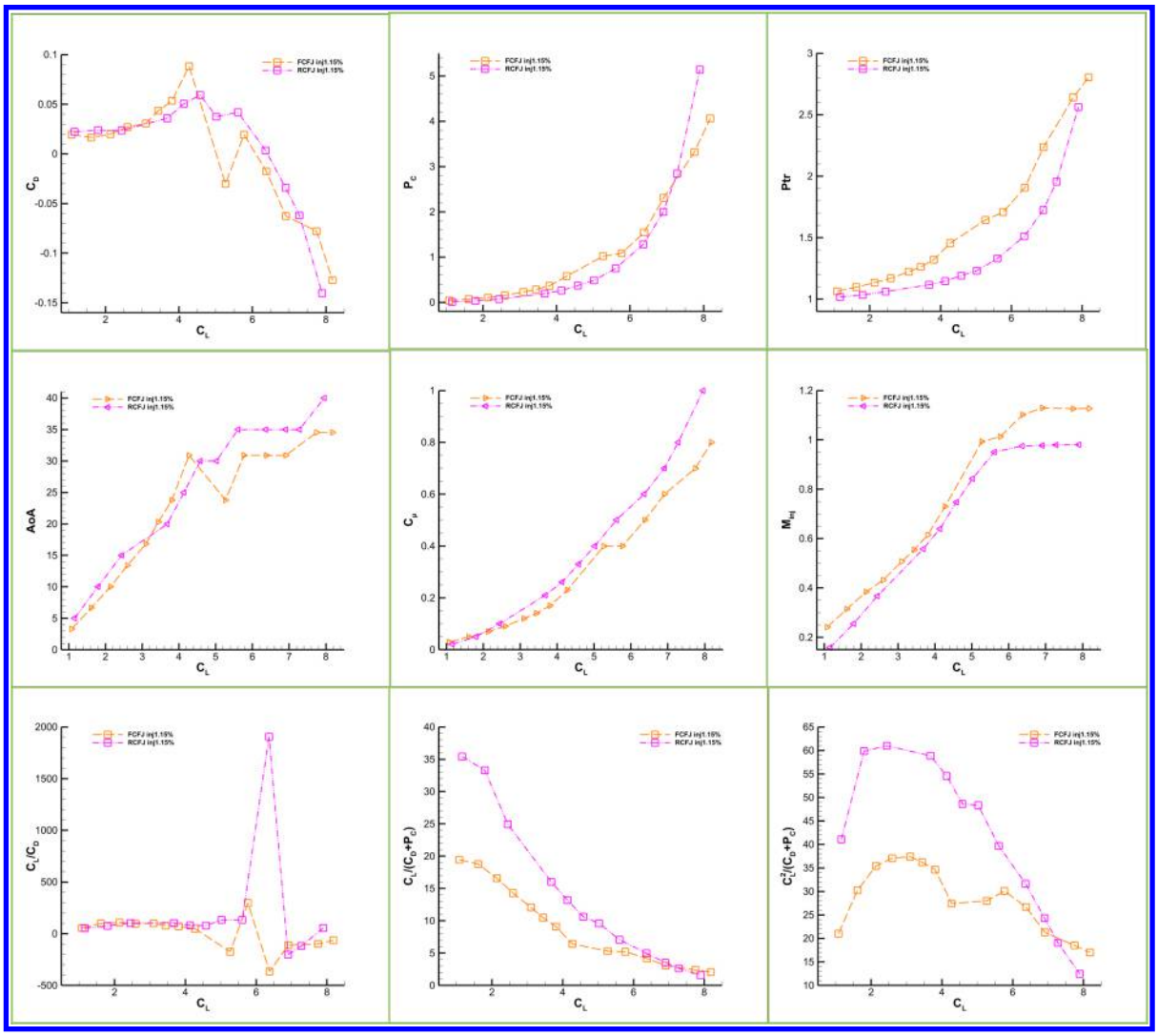

Figure 9: Comparison of C_D, P_c, Ptr, AoA, C_μ, M_{inj}, C_L/C_D, $(C_L/C_D)_c$, $(C_L^2/C_D)_c$ for RCFJ and FCFJ airfoils with $1.15\%C$ injection slot size at $Re = 56,300$.

Figure. 10 compares the FCFJ airfoil performance for the three injection slot sizes. All three cases achieve a similar C_D. As C_L increases, C_D decreases for all the FCFJ cases, and eventually becomes negative with thrust. The largest slot ($1.15\%C$) reaches negative drag at a slightly lower C_L than the other two cases. The power coefficient P_c shows more dependence on slot size at very high lift conditions. Beyond $C_L \approx 7$, the largest slot benefits from the larger slot size with lower total pressure ratio, which affects the power coefficient exponentially [34, 35].

All three slots reach their maximum $(C_L/C_D)_c$ of about 22 at $C_L \approx 1.5$ as shown in Fig. 10, with the $0.4\%C$ and $0.65\%C$ cases giving very similar peak values and the $1.15\%C$ slot slightly lower. The productivity efficiency curves peak around $C_L \approx 3$, where the $0.4\%C$ slot has the highest $(C_L^2/C_D)_c$, and the $1.15\%C$ slot has the smallest $(C_L^2/C_D)_c$. As C_L increases beyond about 5, the corrected aerodynamic efficiency and productivity efficiency of all three cases decrease and gradually converge.

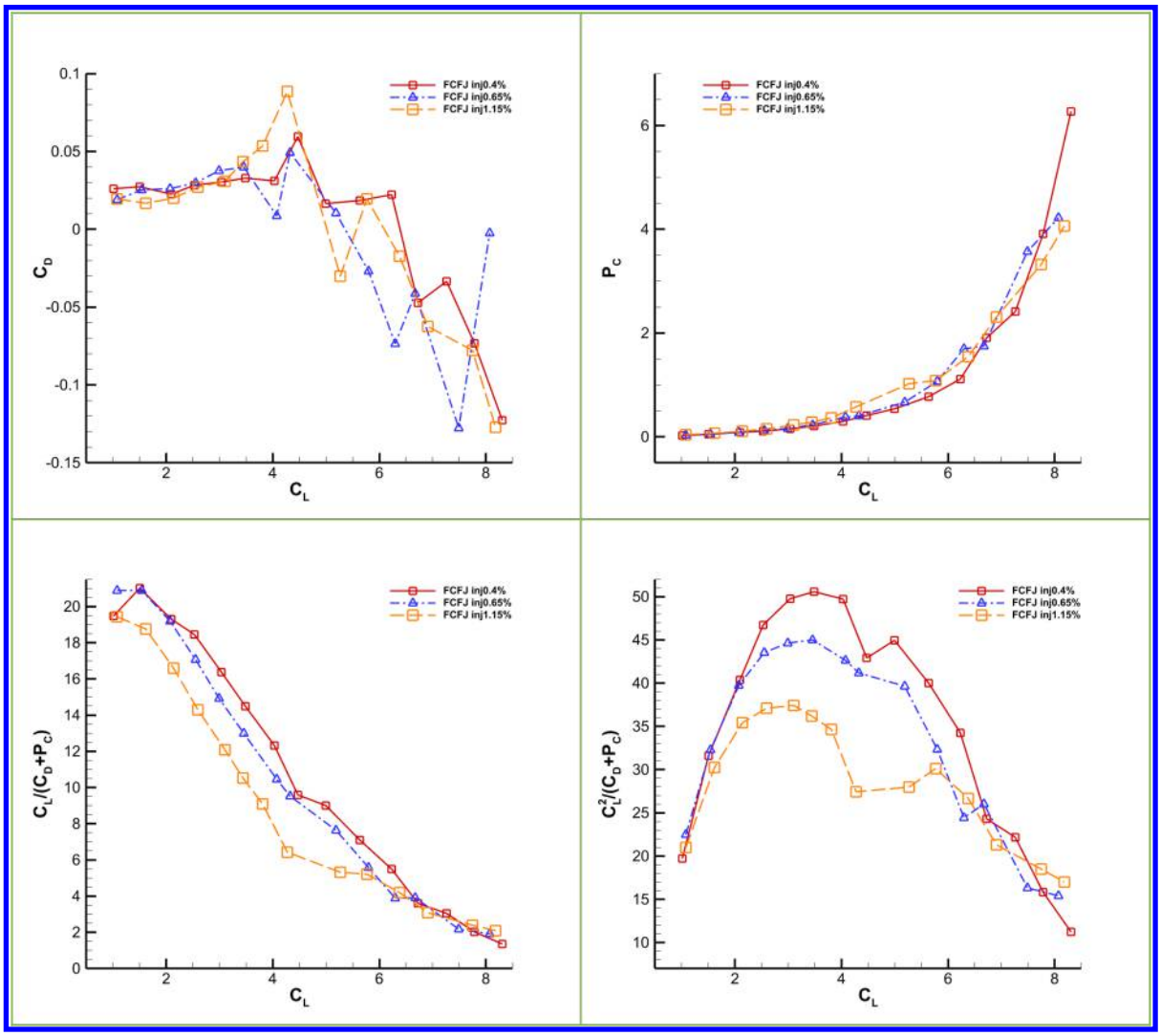

Figure 10: Comparison of C_D, P_c, $(C_L/C_D)_c$, $(C_L^2/C_D)_c$ for FCFJ airfoil at $Re = 56,300$.

Figure. 11 compares the performance of the RCFJ airfoil for all three injection slot sizes. All the RCFJ airfoils reach a similar maximum lift coefficient of 8.0, with the $0.65\%C$ slot giving a slightly higher C_L at the upper end of the whole range. The power coefficient P_c is almost the same for all slot sizes when $C_L \leq 5$. Beyond this range, P_c grows exponentially with C_L, and the $0.4\%C$ slot requires the highest P_c, while the $1.15\%C$ slot requires the lowest.

Similar to the FCFJ configurations, the maximum $(C_L/C_D)_c$ for RCFJ airfoil occurs at $C_L \approx 1.5$, with the $1.15\%C$ cases providing the highest peak values of $(C_L/C_D)_c = 32.9$, about 50% higher than the FCFJ airfoil. The productivity efficiency curves peak around $C_L \approx 3$, where the $0.65\%C$ slot yields the largest value of $(C_L^2/C_D)_c = 64.4$, about 26% higher than that of the FCFJ airfoil.

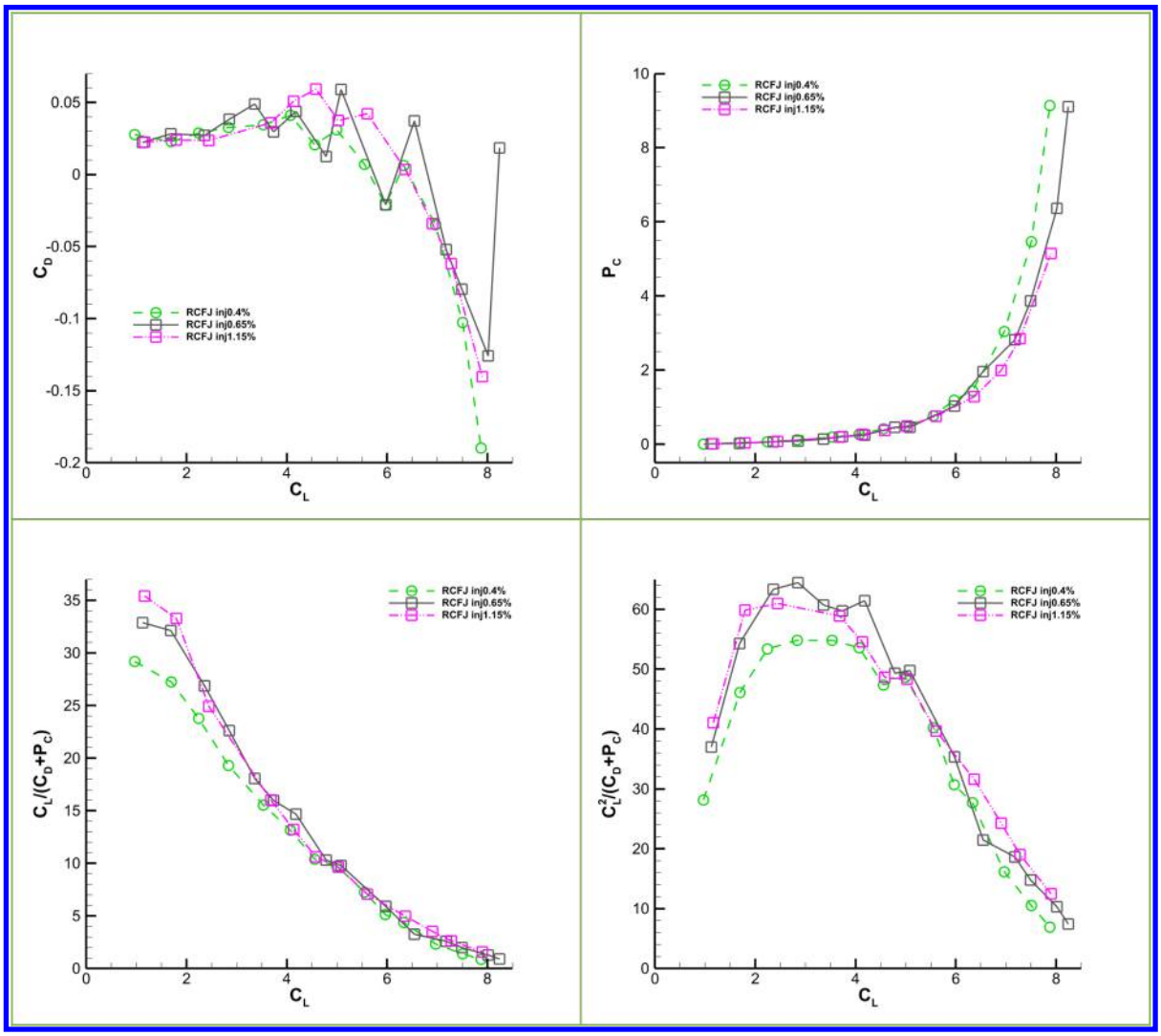

Figure 11: Comparison of C_D, P_c, $(C_L/C_D)_c$, $(C_L^2/C_D)_c$ for RCFJ airfoil at $Re = 56,300$.

4.2 High Reynolds Number Case

Figures 12–14 compare the RCFJ and FCFJ configurations at $Re = 1.0 \times 10^6$ for the three injection slot sizes. Similar to those observed at low Reynolds number, for all three slot sizes, the FCFJ configuration obtains a higher maximum lift coefficient than the RCFJ, while the RCFJ generally shows better power-based aerodynamic efficiency over most of the lift range.

For the $0.4\%C$ slot as shown in Fig. 12, both configurations maintain small drag coefficients up to $C_L \approx 6$, after which C_D drops sharply and becomes negative. The RCFJ airfoil reaches more negative drag than the FCFJ airfoil near its stall point. The power coefficient P_c remains almost identical for both configurations up to $C_L \approx 6$, but beyond this point, the RCFJ airfoil requires much higher power compared with the FCFJ airfoil at the same lift. As a result, at very high lift, the FCFJ airfoil can deliver both higher C_L and lower P_c than the RCFJ airfoil. Compared with the low Reynolds number case, the overall levels of corrected aerodynamic efficiency $(C_L/C_D)_c$ and productivity efficiency $(C_L^2/C_D)_c$ at $Re = 1.0 \times 10^6$ are significantly higher for both configurations. The peak values of $(C_L/C_D)_c$ is increased

from 30 to 61, and $(C_L^2/C_D)_c$ is increased from 55 to 130. This improvement is mainly due to the reduced viscous drag at higher Reynolds numbers. The relative trend between RCFJ and FCFJ configurations remains similar: RCFJ is more efficient at low and moderate C_L, and FCFJ becomes more efficient at the very high-lift regime.

For both $0.65\%C$ and $1.15\%C$ slots, the behavior is similar to the low Reynolds number case. As shown in Fig. 13 and Fig. 14, the corrected aerodynamic efficiency $(C_L/C_D)_c$ and productivity efficiency $(C_L^2/C_D)_c$ of the RCFJ airfoil remain higher across almost the whole lift range for these two slot sizes. However, similar to the $0.4\%C$ case, the peak values of $(C_L/C_D)_c$ and $(C_L^2/C_D)_c$ at $Re = 1.0 \times 10^6$ are substantially higher than those at low Reynolds number by 98% and 100% respectively for both configurations.

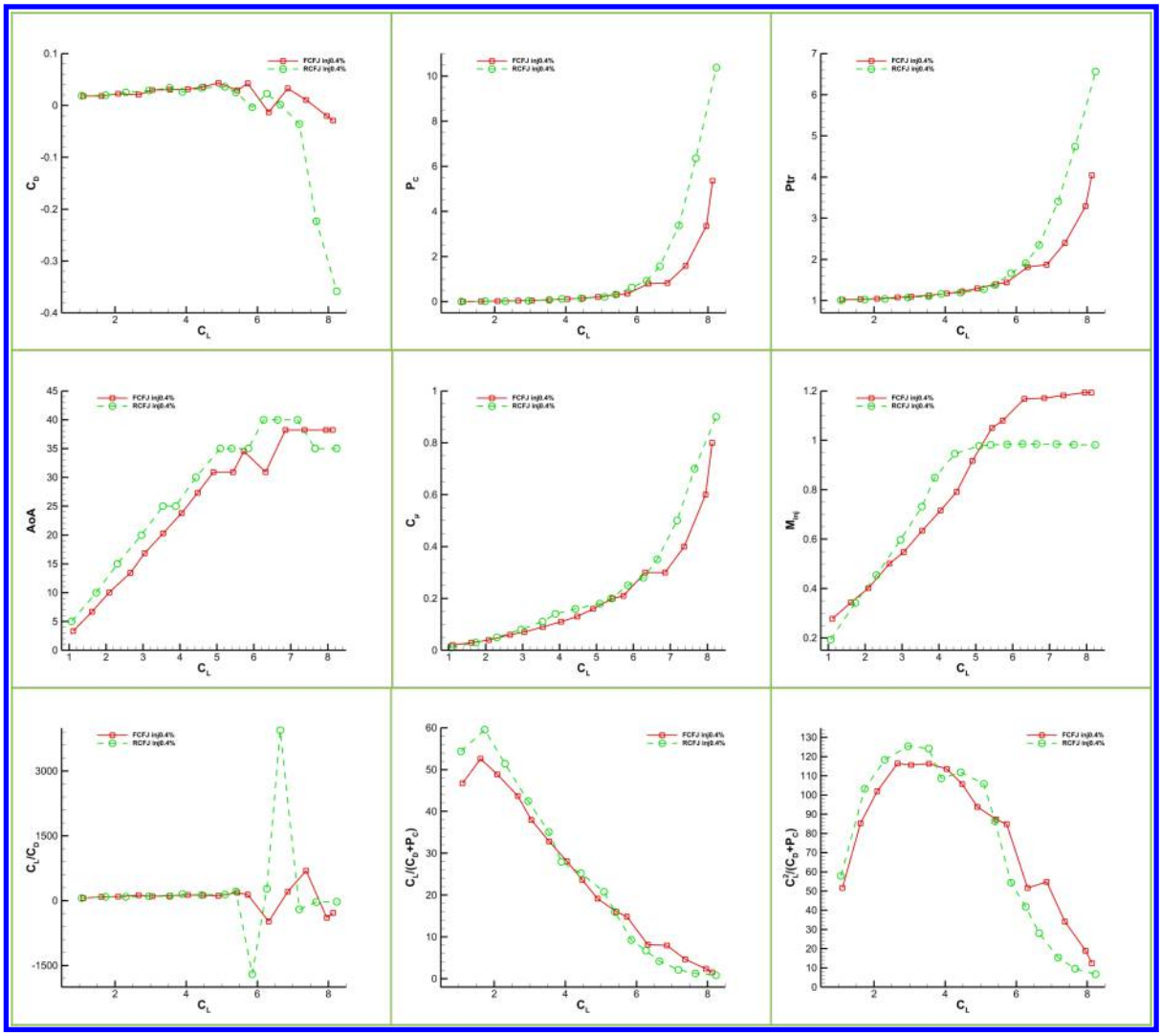

Figure 12: Comparison of C_D, P_c, Ptr, AoA, C_μ, M_{inj}, C_L/C_D, $(C_L/C_D)_c$, $(C_L^2/C_D)_c$ for RCFJ and FCFJ airfoils with $0.4\%C$ injection slot size at $Re = 1 \times 10^6$

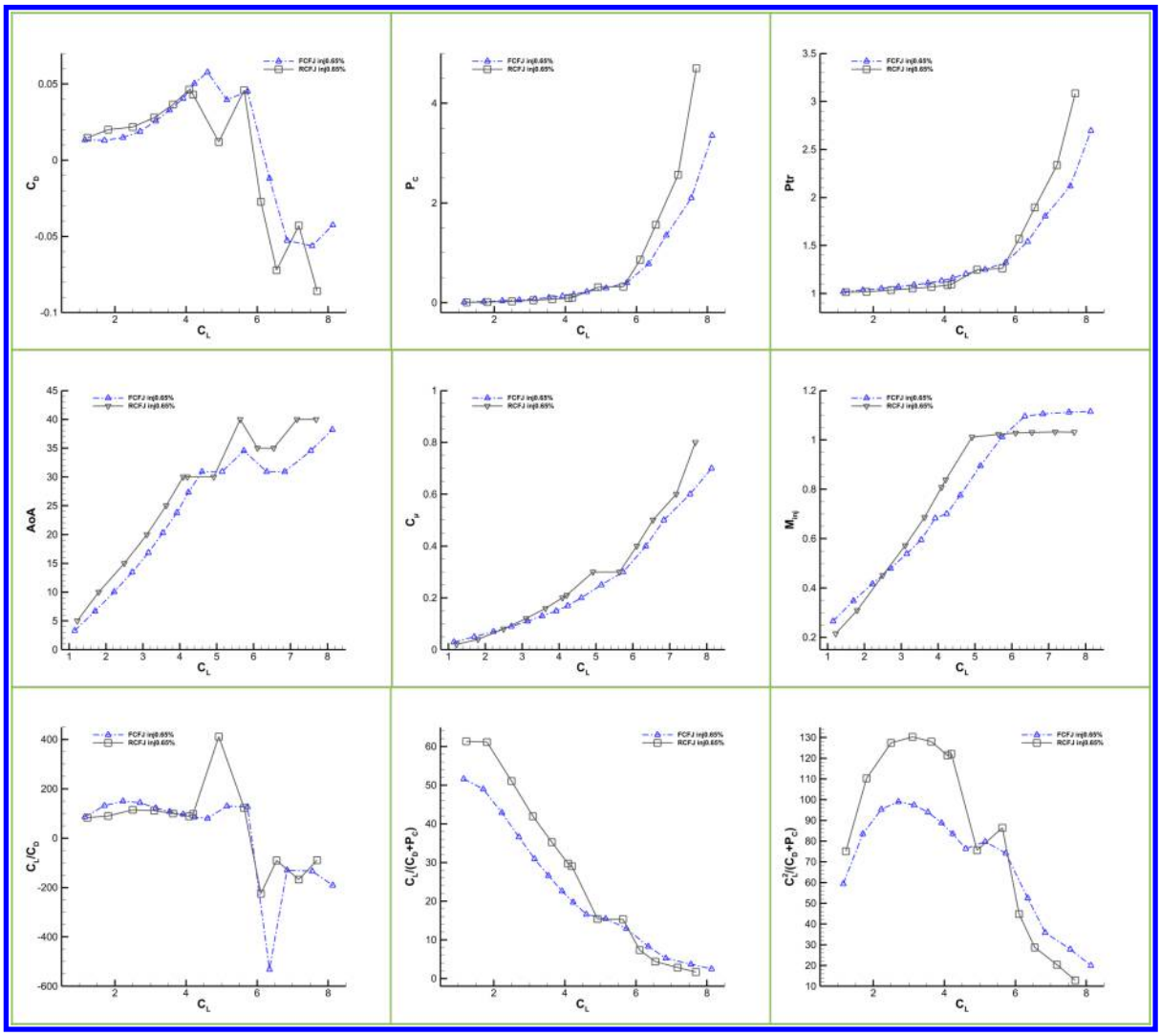

Figure 13: Comparison of C_D, P_c, Ptr, AoA, C_μ, M_{inj}, C_L/C_D, $(C_L/C_D)_c$, $(C_L^2/C_D)_c$ for RCFJ and FCFJ airfoils with $0.65\%C$ injection slot size at $Re = 1 \times 10^6$

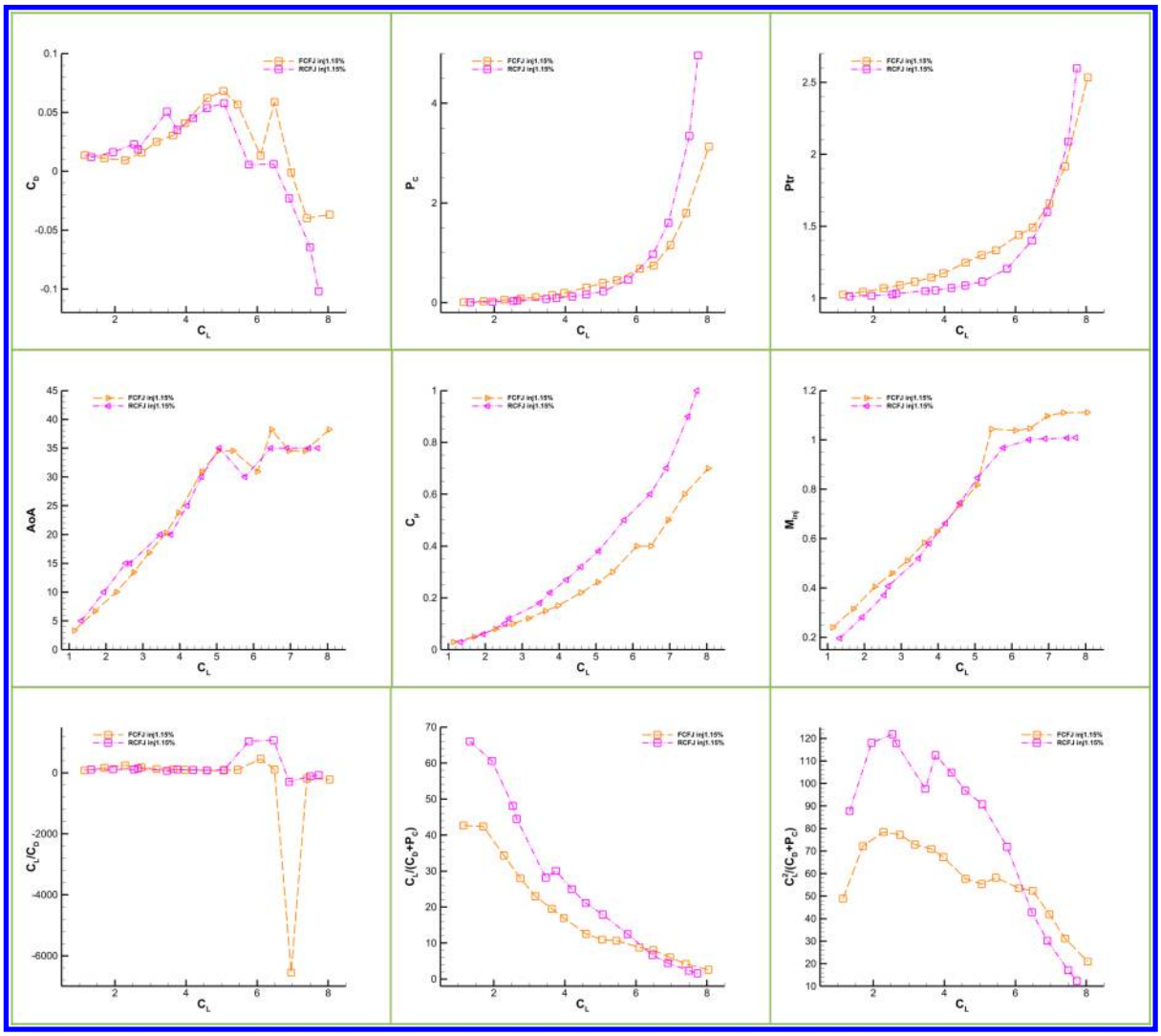

Figure 14: Comparison of C_D, P_c, Ptr, AoA, C_μ, M_{inj}, C_L/C_D, $(C_L/C_D)_c$, $(C_L^2/C_D)_c$ for RCFJ and FCFJ airfoils with 1.15%C injection slot size at $Re = 1 \times 10^6$

At the high Reynolds number condition, the injection slot size has a stronger effect on the corrected aerodynamic efficiencies, especially for the FCFJ configuration. As shown in Fig. 15, the peak productivity efficiency $(C_L^2/C_D)_c$ of the FCFJ airfoil with the 0.4%C slot is roughly 18% and 30% higher than that of the 0.65%C and 1.15%C slot, respectively.

Compared with the low Reynolds number results, the overall trend of $(C_L^2/C_D)_c$ is similar, but the maximum value for all three FCFJ airfoil slots nearly doubled. The RCFJ configuration, shown in Fig. 16, exhibits a weaker dependence on slot size: the three RCFJ airfoil cases achieve very similar peak $(C_L^2/C_D)_c$, with differences within about 10%. The high-Re peaks of $(C_L^2/C_D)_c$ are roughly 100% larger than their low-Re cases.

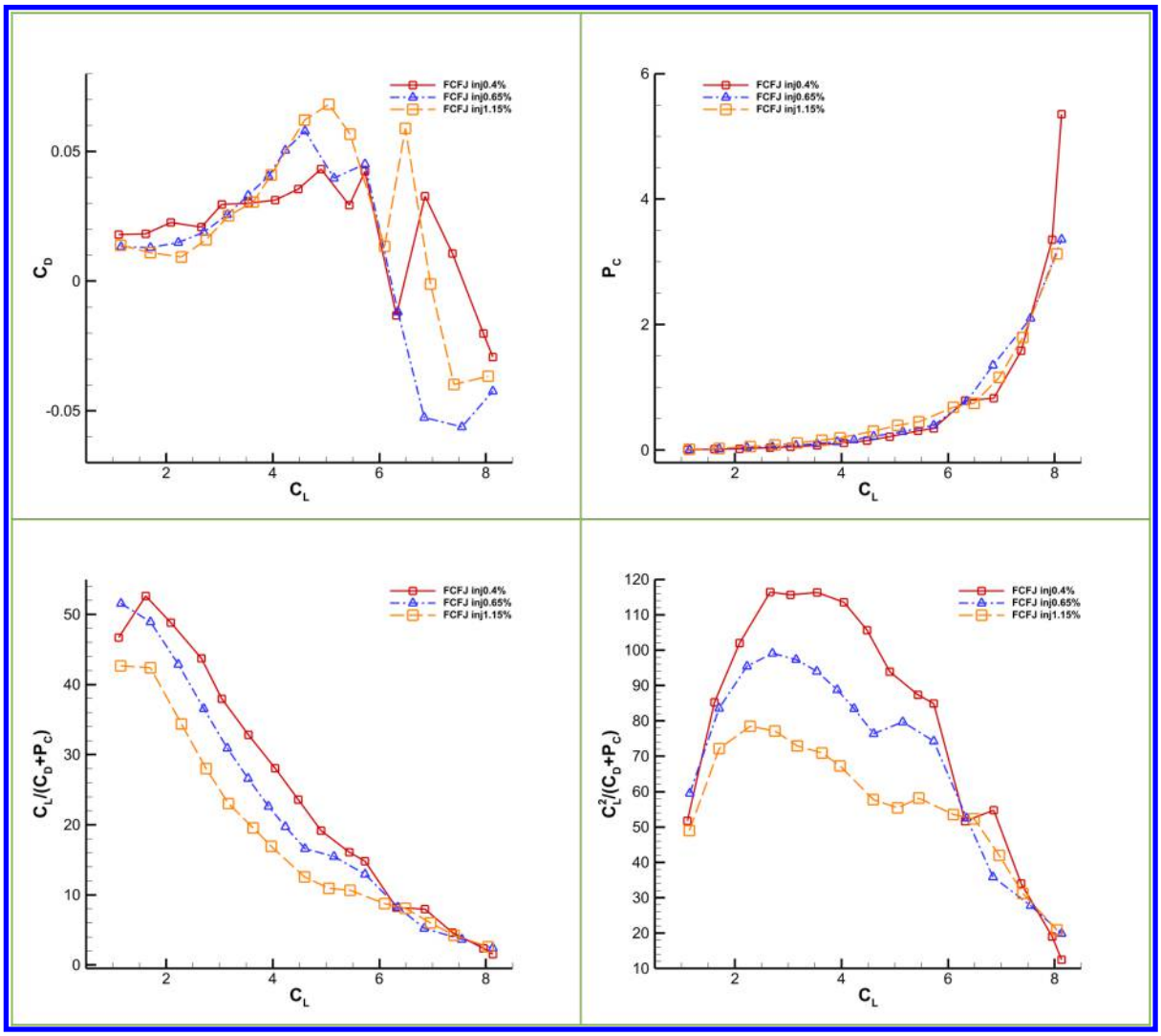

Figure 15: Comparison of C_D, P_c, $(C_L/C_D)_c$, $(C_L^2/C_D)_c$ for FCFJ airfoil at $Re = 1 \times 10^6$.

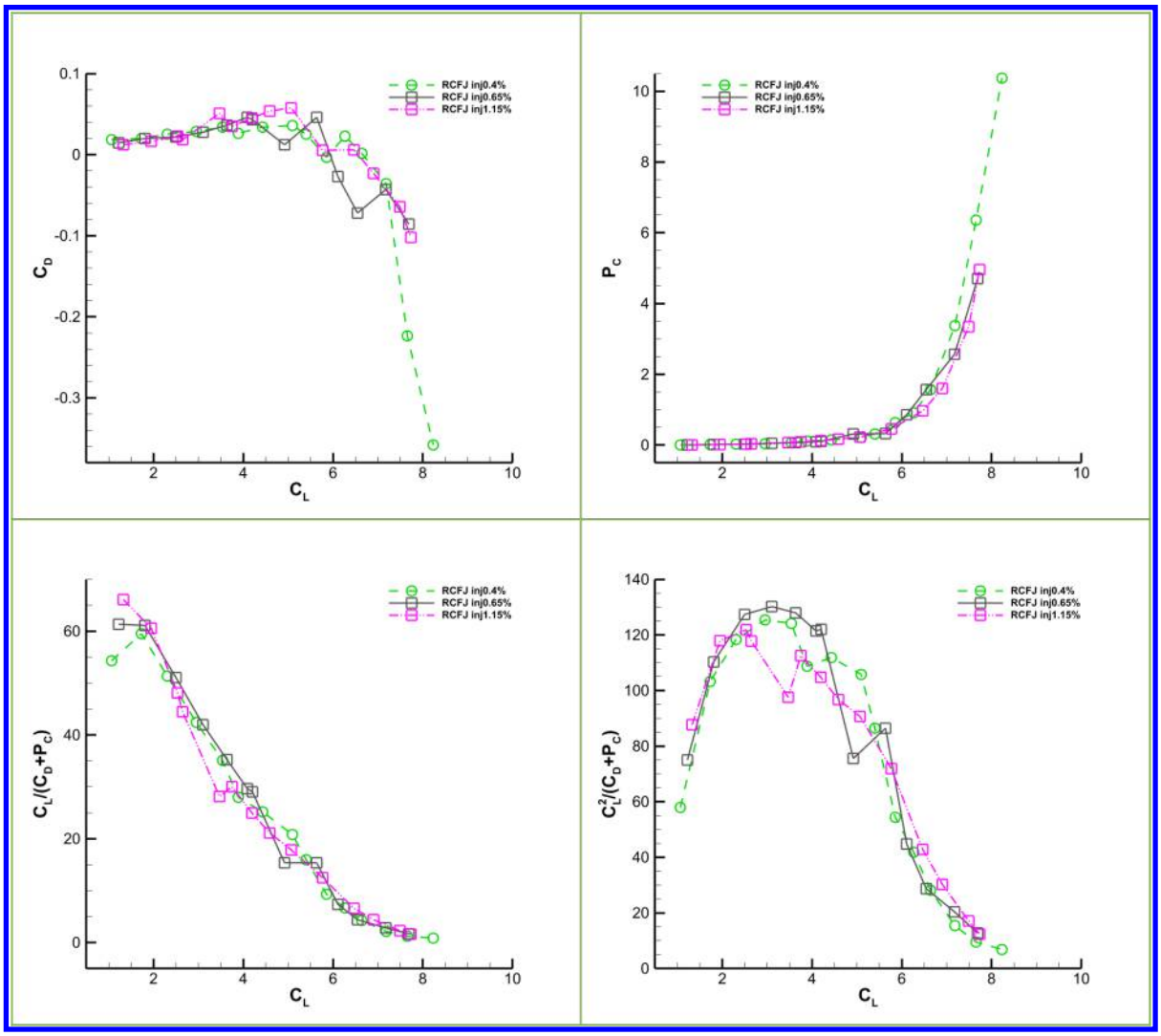

Figure 16: Comparison of C_D, P_c, $(C_L/C_D)_c$, $(C_L^2/C_D)_c$ for RCFJ airfoil at $Re = 1 \times 10^6$.

5 Conclusion

The RCFJ configuration showed better performance over most of the lift range. For $C_L \leq 7$, the RCFJ airfoils exhibited lower drag coefficient C_D and lower power coefficient P_c than the corresponding FCFJ cases, resulting in higher corrected aerodynamic efficiency $(C_L/C_D)_c$ and productivity efficiency $(C_L^2/C_D)_c$. Beyond $C_L \approx 5$ for the $0.4\%C$ slot and $C_L \approx 7$ for the $0.65\%C$ and $1.15\%C$ slots, the FCFJ configuration has a higher $(C_L/C_D)_c$ and $(C_L^2/C_D)_c$ than that of the RCFJ airfoil, indicating that the FCFJ airfoil is more efficient in the high-lift regime. When the injection slot is choked with the injection Mach number of 1 or greater, the CFJ power coefficient is increased exponentially with C_L due to the rapidly increased jet total pressure ratio to overcome the high energy loss at high injection speed.

For the FCFJ airfoils at low Reynolds number, the $0.4\%C$ slot provides the highest peak productivity efficiency, while the $1.15\%C$ slot became advantageous only at very high C_L. For the RCFJ airfoils, all three slots produced similar $C_{L,\max}$. At $Re = 1.0 \times 10^6$, the overall trends with slot size remained the

same as at low Reynolds number, but the peak values of $(C_L/C_D)_c$ and $(C_L^2/C_D)_c$ for both configurations are increased by roughly 100%.

In summary, the RCFJ airfoil is more suitable for low to moderate C_L (e.g., $C_L < 5$) operation, providing higher corrected aerodynamic efficiency and productivity efficiency over a broad range of slot sizes and Reynolds numbers. The FCFJ airfoil provides higher efficiency at a high C_L range.

This paper is the first part of a two-part study. In Part II, the CFJ geometry will be further refined in two ways. First, for the FCFJ configuration, the injection slot location will be shifted closer to the flap shoulder to better align the jet with the inception point of APG and further enhance its high-lift performance. Second, for both RCFJ and FCFJ airfoils, the suction slot inlet angle will be modified to reduce drag and total pressure loss.

6 Acknowledgment

The authors would like to acknowledge the teaching assistantship support from the University of Miami. The computing resource is provided by CoFLow Jet, LLC.

Disclosure: The University of Miami and Dr. Gecheng Zha may receive royalties for future commercialization of the intellectual property used in this study. The University of Miami is also an equity owner in CoFlow Jet, LLC, licensee of the intellectual property used in this study.

References

[1] ZHA, G. and REN, Y. and FREDERICKS, W. , " Design and Testing of Deflected Slipstream Airfoil for VTOL Hover Enabled by CoFlow Jet ," in *AIAA AVIATION FORUM AND ASCEND 2024* , (Las Vegas, Nevada), 29 July–2 August 2024. AIAA Paper 2024-4420 .

[2] Gecheng Zha, Yan Ren, Miranda Anhalzer, Michael A. Mischna, Michael M. Sori, "Mars Aerial and Ground Global Intelligent Explorer (MAGGIE): Mission Feasibility Study," *Proceedings of AIAA SciTech Forum 2026, 12 January 2026 - 16 January 2026, Orlando, FL*, 2026.

[3] G.-C. Zha and D. C. Paxton, "A Novel Flow Control Method for Airfoil Performance Enhancement Using Co-Flow Jet." *Applications of Circulation Control Technologies*, Chapter 10, p. 293-314, Vol. 214, Progress in Astronautics and Aeronautics, AIAA Book Series, Editors: Joslin, R. D. and Jones, G.S., 2006.

[4] G.-C. Zha, W. Gao, and C. Paxton, "Jet Effects on Co-Flow Jet Airfoil Performance," *AIAA Journal, No. 6,*, vol. 45, pp. 1222–1231, 2007.

[5] G.-C. Zha, C. Paxton, A. Conley, A. Wells, and B. Carroll, "Effect of Injection Slot Size on High Performance Co-Flow Jet Airfoil," *AIAA Journal of Aircraft*, vol. 43, 2006.

[6] G.-C. Zha, B. Carroll, C. Paxton, A. Conley, and A. Wells, "High Performance Airfoil with Co-Flow Jet Flow Control," *AIAA Journal*, vol. 45, 2007.

[7] Wang, B.-Y. and Haddoukessouni, B. and Levy, J. and Zha, G.-C., "Numerical Investigations of Injection Slot Size Effect on the Performance of Co-Flow Jet Airfoil," *Journal of Aircraft*, vol. Vol. 45, No. 6,, pp. pp.2084–2091, 2008.

[8] B. P. E. Dano, D. Kirk, and G.-C. Zha, "Experimental Investigation of Jet Mixing Mechanism of Co- Flow Jet Airfoil." AIAA-2010-4421, 5th AIAA Flow Control Conference, Chicago, IL, 28 Jun - 1 Jul 2010.

[9] B. P. E. Dano, G.-C. Zha, and M. Castillo, "Experimental Study of Co-Flow Jet Airfoil Performance Enhancement Using Micro Discreet Jets." AIAA Paper 2011-0941, 49th AIAA Aerospace Sciences Meeting, Orlando, FL, 4-7 January 2011.

[10] A. Lefebvre, B. Dano, W. Bartow, M. Fronzo, and G. Zha, "Performance and energy expenditure of coflow jet airfoil with variation of mach number," *Journal of Aircraft*, vol. 53, no. 6, pp. 1757–1767, 2016.

[11] A. Lefebvre, G-C. Zha, "Numerical Simulation of Pitching Airfoil Performance Enhancement Using Co-Flow Jet Flow Control," *AIAA paper 2013-2517*, June 2013.

[12] A. Lefebvre, G-C. Zha, "Co-Flow Jet Airfoil Trade Study Part I : Energy Consumption and Aerodynamic Performance," *Proceedings of the AIAA Flow Control Conference*, June 2014.

[13] A. Lefebvre, G-C. Zha, "Co-Flow Jet Airfoil Trade Study Part II : Moment and Drag," *Proceedings of the AIAA Flow Control Conference*, June 2014.

[14] Yunchao Yang, Gecheng Zha, "Super-Lift Coefficient of Active Flow Control Airfoil: What is the Limit?," *AIAA Paper 2017-1693, AIAA SCITECH2017, 55th AIAA Aerospace Science Meeting, Grapevine, Texas, 9-13 January 2017*, 2017.

[15] Gecheng Zha, Yunchao Yang, Yan Ren, Brendan McBreen, "Super-Lift and Thrusting Airfoil of Coflow Jet Actuated by Micro-Compressors," *AIAA Paper-2018-3061, AIAA AVIATION Forum 2018, Flow Control Conference, June 25-29*, 2018.

[16] Lefebvre, A. and Zha, G.-C., "Trade Study of 3D Co-Flow Jet Wing for Cruise Performance." AIAA Paper 2016-0570, AIAA SCITECH2016, AIAA Aerospace Science Meeting, San Diego, CA, 4-8 January 2016.

[17] Kewei Xu, Gecheng Zha, "High Control Authority 3D Aircraft Control Surfaces Using Co-Flow Jet," *AIAA Journal of Aircraft*, 2020.

[18] Kewei Xu, Yan Ren, Gecheng Zha, "Numerical Analysis of Energy Expenditure for Co-Flow Wall Jet Separation Control," *AIAA Journal, published online: 11 Jan 2022, doi.org/10.2514/1.J061015*, 2022.

[19] Kewei Xu, Yan Ren, and Gecheng Zha, "Analysis of separation control mechanism of turbulent coflow wall jet," *Elsevier Journal of Aerospace Science and Technology*, vol. 110775, pp. 110775, DOI: https://doi.org/10.1016/j.ast.2025.110775, 2026.

[20] Zha, G.-C,, "Feasibility Study of Deflected Slipstream Airfoil for VTOL Hover Enabled by CoFlow Jet," *Proceedings of AIAA Aviation Forum 2023, 12–16 June 2023, San Diego, CA*, 2023.

[21] Jeon, Jaehyoung and Ren, Yan and Zha, Gecheng, "Toward Ultra-high Cruise Lift Coefficient Using Flapped Coflow Jet Airfoil," *AIAA Paper 2023-1008, AIAA AVIATION 2023 Forum*, 2023.

[22] Y.-Q. Shen and G.-C. Zha, "Large Eddy Simulation Using a New Set of Sixth Order Schemes for Compressible Viscous Terms ," *Journal of Computational Physics*, vol. 229, pp. 8296–8312, 2010.

[23] Zha, G.C., Shen, Y.Q. and Wang, B.Y., "An improved low diffusion E-CUSP upwind scheme ," *Journal of Computer and Fluids*, vol. 48, pp. 214–220, Sep. 2011.

[24] Y.-Q. Shen and G.-Z. Zha , "Generalized finite compact difference scheme for shock/complex flowfield interaction," *Journal of Computational Physics*, vol. doi:10.1016/j.jcp.2011.01.039, 2011.

[25] Shen, Y.-Q. and Zha, G.-C. and Wang, B.-Y., " Improvement of Stability and Accuracy of Implicit WENO Scheme," *AIAA Journal*, vol. 47, No. 2, pp. 331–344, 2009.

[26] Shen, Y.-Q. and Zha, G.-C. and Chen, X.-Y., " High Order Conservative Differencing for Viscous Terms and the Application to Vortex-Induced Vibration Flows," *Journal of Computational Physics*, vol. 228(2), pp. 8283–8300, 2009.

[27] Shen, Y.-Q. and Zha, G.-C. , " Improvement of the WENO Scheme Smoothness Estimator," *International Journal for Numerical Methods in Fluids*, vol. DOI:10.1002/fld.2186, 2009.

[28] G.-C. Zha and E. Bilgen, "Numerical Study of Three-Dimensional Transonic Flows Using Unfactored Upwind-Relaxation Sweeping Algorithm," *Journal of Computational Physics*, vol. 125, pp. 425–433, 1996.

[29] B.-Y. Wang and G.-C. Zha, "A General Sub-Domain Boundary Mapping Procedure For Structured Grid CFD Parallel Computation," *AIAA Journal of Aerospace Computing, Information, and Communication*, vol. 5, No.11, pp. 2084–2091, 2008.

[30] Wang, B. Y and Zha, G.-C. , "Detached-Eddy Simulation of a Co-Flow Jet Airfoil at High Angle of Attack." AIAA Paper 2009-4015, accepted for publication in Journal of Aircraft, 2011.

[31] Im, H.-S. and Zha, G.-C. and Dano, B. P. E., "Large Eddy Simulation of Coflow Jet Airfoil at High Angle of Attack," *Journal of Fluid Engineering, vol. 136(2), p. 021101*, 2014.

[32] Lefebvre, A. and Dano, B. and Bartow, W. and Di Franzo, M. and Zha, G.-C., "Performance Enhancement and Energy Expenditure of Co-Flow Jet Airfoil with Variation of Mach Number." AIAA Paper 2013-0490, AIAA Journal of Aircraft, DOI: 10.2514/1.C033113, 2016.

[33] Y.-Q. Shen, G.-C. Zha, and B.-Y. Wang, "Improvement of Stability and Accuracy of Implicit WENO Scheme ," *AIAA Journal*, vol. 47, pp. 331–344, 2009.

[34] Yang Wang, Yunchao Yang and Gecheng Zha, "Study of Super-Lift Coefficient of Co-Flow Jet Airfoil and Its Power Consumption," *AIAA Paper 2019-3652, AIAA Aviation 2019 Forum, 17-21 June 2019, Dallas, Texas* , 2019.

[35] Yang Wang and Gecheng Zha, "Study of 3D Co-flow Jet Wing Induced Drag and Power Consumption at Cruise Conditions," *AIAA Paper 2019-0034, AIAA SciTech 2019 Forum, 7-11 January 2019, San Diego, CA*, 2019.